

**IMAGE PROCESSING SCHEME FOR
SINGLE PIXEL IMAGING**

NG JIAN HAU


**A project report submitted in partial fulfilment of the
requirements for the award of Bachelor of Engineering
(Honours) Electrical and Electronic Engineering**

**Lee Kong Chian Faculty of Engineering and Science
Universiti Tunku Abdul Rahman**

May 2021

DECLARATION

I hereby declare that this project report is based on my original work except for citations and quotations which have been duly acknowledged. I also declare that it has not been previously and concurrently submitted for any other degree or award at UTAR or other institutions.

Signature :  _____

Name : Ng Jian Hau _____


ID No. : 1604762 _____

Date : 6May2021 _____

APPROVAL FOR SUBMISSION

I certify that this project report entitled “**IMAGE PROCESSING SCHEME FOR SINGLE PIXEL IMAGING**” was prepared by **NG JIAN HAU** has met the required standard for submission in partial fulfilment of the requirements for the award of Bachelor of Engineering (Honours) Electrical and Electronic Engineering at Universiti Tunku Abdul Rahman.

Approved by,

Signature : 

Supervisor : Chua Sing Yee

Date : 10 May 2021

Signature : _____
Co-Supervisor : _____
Date : _____

The copyright of this report belongs to the author under the terms of the copyright Act 1987 as qualified by Intellectual Property Policy of Universiti Tunku Abdul Rahman. Due acknowledgement shall always be made of the use of any material contained in, or derived from, this report.

© 2021, Ng Jian Hau. All right reserved.

ACKNOWLEDGEMENTS

I would like to thank everyone who had contributed to the successful completion of this project. I would like to express my gratitude to my research supervisor, Dr. Chua Sing Yee for her invaluable advice, guidance and her enormous patience throughout the development of the research.

In addition, I would also like to express my gratitude to my loving parents and friends who had helped and given me encouragement throughout the entire project.

ABSTRACT

Single pixel imaging is substantially different from conventional imaging approaches which it needs only a bucket detector to capture images instead of a pixelated detector. It has been a promising method for imaging with non-visible light, imaging through turbid media and weak-light conditions. Compressed sensing is commonly used in single pixel imaging to efficiently acquire and reconstruct signals with less than Nyquist sampling rate. Same resolution grade of masks formed by Pseudorandom or Hadamard matrix are used to sample information from the target scene. Image can be reconstructed by computational means based on the sample measurements. However, this technique is not adequate to produce a high-quality image which remains the major drawback. Therefore, this project aims to propose a suitable image processing scheme to achieve better image quality. Two approaches are proposed to improve the overall image quality; a Coarse-to-Fine sampling method in the data acquisition phase and Super Resolution enhancement in the post-image reconstruction phase. To realize the Coarse-to-Fine sampling, a sequence of masks with increasing resolution grade from low to high are used to capture different outline information. As for Super Resolution enhancement, a network formed using deep learning approach named Very Deep Super Resolution (VDSR) is used to estimate the information loss in the low resolution image. In general, the proposed Coarse-to-Fine sampling and VDSR method show improvement in image quality. Integrated scheme by combining both proposed methods is proven to outperform the conventional compressive sensing especially from the perspective of structural similarity index measurement (SSIM).

TABLE OF CONTENTS

DECLARATION		i
APPROVAL FOR SUBMISSION		ii
ACKNOWLEDGEMENTS		iv
ABSTRACT		v
TABLE OF CONTENTS		vi
LIST OF TABLES		viii
LIST OF FIGURES		ix
LIST OF SYMBOLS / ABBREVIATIONS		xi
CHAPTER		
1	INTRODUCTION	1
1.1	General Introduction	1
1.2	Importance of the Study	1
1.3	Problem Statement	2
1.4	Aim and Objectives	2
1.5	Scope and Limitation of the Study	3
1.6	Contribution of the Study	3
1.7	Outline of the Report	3
2	LITERATURE REVIEW	5
2.1	Single Pixel Imaging	5
2.2	Digital Microscanning	6
2.2.1	Normal High Resolution Convolved	6
2.2.2	Complete Microscanning	7
2.2.3	Quarter Microscanning	7
2.3	Compressed Sensing	8
2.3.1	Basic Framework	8
2.3.2	Data Acquisition Mechanism	10
2.4	Image Processing Techniques	11
2.4.1	Super Resolution	11

	2.4.2	Image interpolation	14
	2.5	Summary	16
3		METHODOLOGY AND WORK PLAN	17
	3.1	Introduction	17
	3.2	Data Acquisition	19
	3.2.1	Coarse-to-Fine Sampling Method	20
	3.3	Image Post-processing Technique	21
	3.3.1	Image interpolation	21
	3.3.2	Very Deep Super Resolution	21
	3.4	Proposed Integration of Image Acquisition and Post-processing Scheme	23
	3.5	Evaluation Methods	23
	3.5.1	Peak Signal-to-Noise Ratio (PSNR)	24
	3.5.2	Structural Similarity Index Measurement (SSIM)	25
	3.5.3	Root Mean Square Error (RMSE)	25
	3.5.4	Statistical Test	26
4		RESULTS AND DISCUSSION	27
	4.1	Data Acquisition Phase	27
	4.1.1	Hadamard Mask	27
	4.1.2	Pseudorandom Mask	28
	4.1.3	Discussion	29
	4.2	Post-processing Phase	29
	4.3	Proposed Integration of Image Acquisition and Post-processing Scheme	32
	4.3.1	Hadamard Mask	32
	4.3.2	Pseudorandom Mask	35
	4.3.3	Discussion	38
5		CONCLUSION AND RECOMMENDATION	39
	5.1	Conclusion	39
	5.2	Recommendation for Future Work	39
		REFERENCES	40
		APPENDICES	43

LIST OF TABLES

Table 4.1: Quantitative comparison between the normal compressed sensing and Coarse-to-Fine (c2f) sampling method using Hadamard mask. Highlighted results indicate the best performance.	27
Table 4.2: Quantitative comparison between normal compressed sensing and Coarse-to-Fine (c2f) sampling method using Pseudorandom mask. Highlighted results indicate the best performance.	28
Table 4.3: Quantitative comparison between different interpolation methods and super resolution using the reconstructed images from Hadamard mask. Highlighted results indicate the best performance.	30
Table 4.4: Quantitative comparison between different interpolation methods and super resolution using the reconstructed images from Pseudorandom mask. Highlighted results indicate the best performance.	31
Table 4.5: Quantitative comparison between different method implemented using Hadamard masks. A) Conventional compressed sensing, B) Coarse-to-Fine sampling method, C) Very Deep Super Resolution (VDSR), and D) Proposed integration method. Highlighted results indicate the best performance.	34
Table 4.6: Quantitative comparison between different method implemented using Pseudorandom masks. A) Conventional compressed sensing, B) Coarse-to-Fine sampling method only, C) Very Deep Super Resolution (VDSR) only, and D) Proposed integration method. Highlighted results indicate the best performance.	37

LIST OF FIGURES

Figure 2.1: Example of a single pixel imaging system (Phillips <i>et al.</i> , 2017)	5
Figure 2.2: Overall process of complete microscanning method (Sun <i>et al.</i> , 2016)	7
Figure 2.3: Schematics diagram of two digital microscanning method. a) Complete microscanning. b) Quarter microscanning. (Sun <i>et al.</i> , 2016)	8
Figure 2.4: Illustration of compressed sensing equation. a) In Φ and Ψ form. b) In Θ form. (Baraniuk, 2007)	9
Figure 2.5: Aliasing relationship between DFT and CFT (Makwana and Mehta, 2013).	12
Figure 2.6: Result of the nearest neighbor interpolation algorithm (Howard, 2018).	14
Figure 2.7: Result of the bilinear interpolation algorithm (Understanding Digital Image Interpolation, 2021).	15
Figure 2.8: Result of the bicubic interpolation algorithm (Understanding Digital Image Interpolation, 2021).	15
Figure 3.1: Flow diagram of single pixel image processing.	17
Figure 3.2: Gantt chart of the project for first semester.	18
Figure 3.3: Gantt chart of the project for second semester.	18
Figure 3.4: Work plan of the project.	19
Figure 3.5: Sample of masks with a same resolution grade used for data acquisition.	20
Figure 3.6: Sample of masks with an increasing resolution grade (from left to right).	20
Figure 3.7: a) High resolution image. b) Low resolution image. c) Residual image.	22
Figure 3.8: Illustration of the proposed system overview.	23

Figure 4.1: Qualitative comparison between different method implemented using Hadamard masks. a) Ground truth, b) Conventional compressed sensing, c) Coarse-to- Fine sampling method only, d) Very Deep Super Resolution (VDSR) only, and e) Proposed integration method.

33

Figure 4.2: Qualitative comparison between different method implemented using Pseudorandom masks. a) Ground truth, b) Conventional compressed sensing, c) Coarse-to- Fine sampling method only, d) Very Deep Super Resolution (VDSR) only, and e) Proposed integration method.

36

LIST OF SYMBOLS / ABBREVIATIONS

Φ	measurement matrix
Ψ	orthonormal basis space
Θ	coding pattern
u	learning factor
AC	Analytic Continuation
AI	Artificial Intelligence
ANN	Artificial Neural Network
BP	Basic Pursuit
CCD	Charged Coupled Device
CFT	Continuous Fourier Transform
CM	Complete Microscanning
CMOS	Complementary Metal-Oxide Semiconductor
CS	Compressed Sensing
DCT	Discrete Cosine Transform
DFT	Discrete Fourier Transform
DMD	Digital Micro-mirror Device
DWT	Discrete Wavelet Transform
FT	Fourier Transform
HR	High Resolution
LR	Low Resolution
MSE	Mean Square Error
NHRC	Normal High Resolution Convolved
PSNR	Peak Signal-to-Noise Ratio
QM	Quarter Microscanning
RE	Reputation Error
RMSE	Root Mean Square Error
SLP	Single Layer Perceptron
SNR	Signal-to-Noise Ratio
SPI	Single Pixel Imaging
SR	Super Resolution
SSIM	Structural Similarity Index Measurement

SVD	Singular Value Decomposition
TV	Total Variation
VDSR	Very Deep Super Resolution

CHAPTER 1

INTRODUCTION

1.1 General Introduction

Almost in every camera, there is an image sensor function to register the amount of light to convert them into the corresponding number of electrons for image reconstruction (AXIS, 2010). Without a doubt, every camera has image sensors which consist of a different number of pixels that lead to a difference in image quality produced. There are two types of image sensor being widely implemented worldwide which is Charged Coupled Device (CCD) and Complementary Metal-Oxide Semiconductor (CMOS). Both of them have the limitation in spectral bands or wavelength and low sensitivity to low light intensity. To cope with this, the cost of implementation will increase as well. This trade-off had led to the development of a new imaging technology, Single Pixel Imaging (Edgar *et al.*, 2015).

Single Pixel Imaging (SPI) measures the spatial information of the image scene using a high sensitivity photodiode as its image sensor which can capture a broad range of spectral bands. Thus, this emerging technology had successfully attracted the public attention as it can overcome the challenge faced by both the CCD and CMOS, trade-off between cost and spectral range. SPI had been implemented in various applications such as terahertz imaging, ultraviolet and time-correlated single photon counting, multi-wavelength imaging, three-dimensional imaging and many others (Sun and Zhang, 2019).

The commonly used technique in single pixel imaging is compressed sensing. As compared to other techniques, a lesser amount of measurement is needed to acquire and reconstruct the desired signal. However, this technique cannot produce a high-quality of image. Thus, a lot of future work can be done on compressed sensing to improve its practicability in single pixel imaging.

1.2 Importance of the Study

SPI has great potential due to its cost effectiveness and simplicity in the system design. Generally, this system only consists of a light source, Digital Micro-mirror Device (DMD), lens and a photodiode. Conventional imaging

sensors often reach their limits in terms of resolution and dynamic range, especially in unusual spectral bands or wavelengths. On the other hand, single pixel imaging works efficiently across different spectral regions and low light condition. Thus, it provides a cost effective solution as compared to conventional imaging technology.

Therefore, it is crucial to enhance the performance of single pixel imaging to involve its practicality in various applications.

1.3 Problem Statement

Problem statements for the current study of image processing scheme of single pixel imaging are summarized as below:

- In the current digital technology, camera performance relies on the number of pixels used (Kuusela, 2019). Thus, the image quality provided by SPI is not as good as the conventional camera due to the limited number of pixels (measurements) sampled in the system. Large number of measurements required has become the main issue face in SPI (Lyu *et al.*, 2017).
- Random and Hadamard matrix are commonly used as the measurement matrix in SPI. Lack of spatial information obtained by using these measurement matrix lead to a low image quality. Furthermore, the image quality is still directly proportional to the number of measurements (Liu *et al.*, 2020).
- SPI is more computational expensive compared to conventional imaging technique. Image acquisition and reconstruction are the key components which affect the performance of SPI (Edgar, Gibson and Padgett, 2019). Hence, a suitable image processing scheme considering the number of measurements and image quality is needed.

1.4 Aim and Objectives

This project aims to improve the performance of SPI through image processing technique. The detail objectives of this project are to:

- Review the single pixel imaging and image processing algorithms.

- Study on the acquisition and reconstruction of single pixel imaging.
- Propose a suitable image processing scheme to achieve better image quality.

1.5 Scope and Limitation of the Study

This project focuses on the image acquisition and reconstruction of SPI. At the end of this project, it is hoped to develop a suitable image processing scheme for SPI. The performance of proposed scheme was measured in term of the image quality.

Within the scope of this project, a limited sample size was covered but in a number that is adequate for this study. Selected image datasets and measurement matrix were used for data collection and analysis.

1.6 Contribution of the Study

Throughout this project, an image processing scheme is proposed for single pixel imaging using advanced compressed sensing and super resolution with deep learning. The main contributions of the study are as follow:

- Commonly used data acquisition and image post-processing techniques were reviewed and analyzed.
- Coarse-to-Fine sampling method was proposed to replace the existing sampling method.
- Very Deep Super Resolution (VDSR) was used to improve the quality of the final image.
- Coarse-to-Fine sampling method and VDSR were integrated into the SPI flow and was proven to outperform the conventional compressive sensing especially from the perspective of structural similarity index measurement (SSIM).

1.7 Outline of the Report

This report consists of five chapters. The introduction in Chapter 1 gives an overview of single pixel imaging, highlight the problem statement and the aim of the project. Chapter 2 reviews the related works in SPI, background of compressed sensing and image processing techniques. Chapter 3 explains the

work plan for this project and the proposed techniques to improve the performance of the system. The results and discussion in Chapter 4 presents the result obtained throughout the project. Lastly, Chapter 5 concludes the overall performance of the proposed processing scheme for single pixel imaging and possible future work to improve the system.

CHAPTER 2

LITERATURE REVIEW

2.1 Single Pixel Imaging

The main characteristic of Single Pixel Imaging (SPI) is that this technology only utilises a pixel in image processing instead of using millions of pixel array (Sun andZhang, 2019). The pixel here refers to a single light sensitive detector, photodiode. Thus, it is way cheaper as compared to conventional imaging technology such as CCD and CMOS (Duarte *et al.*, 2008). Besides, it is suitable to be implemented in the application which duelling with a low light condition or big spectral range (Jauregui-Sánchez *et al.*, 2018). Moreover, single pixel imaging does provide a better sensing flexibility where its photodiode can have a quantum efficiency of 90% where the conventional camera can only have a maximum of 50% (Baraniuk *et al.*, 2011).

Single pixel imaging measures the spatial information of the target image using a DMD. DMD samples the target image with a series of masks and the photodiode measures the intensity of the light passing through the mask (Edgar, Gibson andPadgett, 2019). The correlation between them is used to reconstruct an image. A simple single pixel imaging system is shown in Figure 2.1.

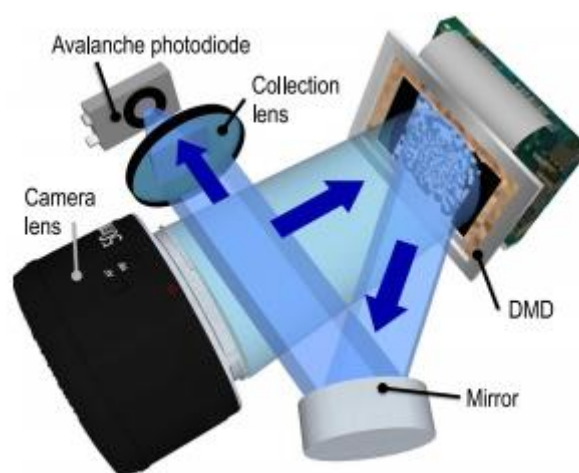


Figure 2.1: Example of a single pixel imaging system (Phillips *et al.*, 2017)

However, SPI has a limitation on producing an image of high quality. This is because in order to reconstruct an ideal image, the number of measurement required to fully sample the target image is directly proportional to the number of pixels. Thus, it led to the development of compressed sensing (Phillips *et al.*, 2017). This technique uses the principle of sparse basis in data acquiring process which requires a lesser amount of measurement for the reconstruction of image. Compressed sensing technique will be further discussed in Section 2.3.

2.2 Digital Microscanning

In the current single pixel imaging system, there are still many limitations which hinder its usage in practical application. The biggest restriction of this system is the low signal-to-noise ratio (SNR) of the image constructed. This becomes worse when the resolution of the image is further increases. The two main sources of noise which affecting the SNR came from illumination noise at mask pattern and detector noise at photodiode (Sun *et al.*, 2016). Thus, digital microscanning is implemented to increase the performance of the single pixel imaging system. The concept of digital microscanning is to obtain a few images with a low resolution which laterally displaced by half a pixel. Then, a high resolution image can be reconstructed by co-registering all the images obtained on a higher resolution grid (Shi *et al.*, 2015). This microscanning approach is applicable to all single pixel imaging system as the modification is carried out on the mask using the DMD.

2.2.1 Normal High Resolution Convolved

The normal high resolution convolved (NHRC) method increases the resolution of the mask used in the DMD without using any imaging technique to obtain a higher resolution image. However, the SNR of the image drops when the number of pixel in mask increases. Although the reconstruction of image includes the convolution with smoothing kernel, the result is still unsatisfying. Thus, Weiner deconvolution algorithm can be implemented when high resolution image is reconstructed using the four sub-pixel shifted images to get a better SNR result.

2.2.2 Complete Microscanning

The complete microscanning (CM) use a total of four low resolution images where the mask of the system is being shifted by a sub-pixel size of translation. The first low resolution image is the original image while the others are shifted in x, y and both xy direction respectively. For example, if one pixel of the mask consists of 192×192 micromirrors, the shifting of half a pixel in x direction will become 192×96 micromirrors and the same goes to the other shifting direction. All the shifting is done on the DMD mirror binning instead of physical shifting in photodiode sensor so that it has higher accuracy on image registration. The four low resolution images are co-register on a higher resolution grid and takes an average of the overlapping pixels to reconstruct a higher resolution image. The result obtained using this method shows a higher SNR as compared to the NHR method when there is a presence of noise such as low light level or else the results are just the same (Sun *et al.*, 2016). Figure 2.2 shows the overall process of CM.

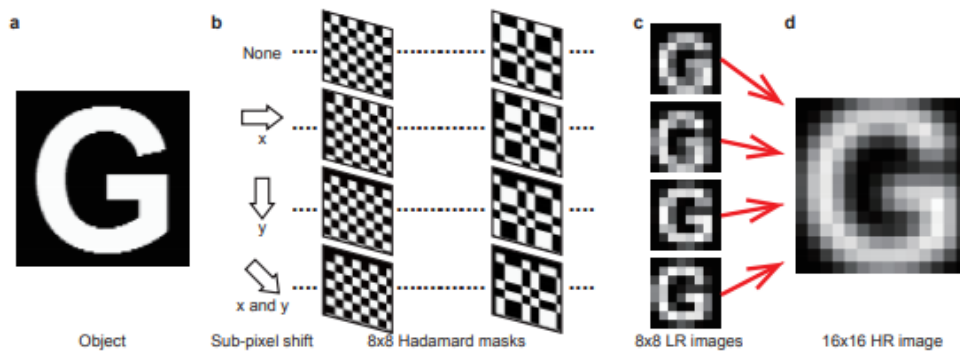


Figure 2.2: Overall process of complete microscanning method (Sun *et al.*, 2016)

2.2.3 Quarter Microscanning

The quarter microscanning (QM) method is similar to CM. The only difference is that a quarter of micromirrors are used per pixel. This means that the pixel is divided into four quadrants and every shifting process only records a quadrant of the image. There will be no overlapping pixel value in reconstructing the high resolution image. Thus, if there is a presence of noise, the SNR will drop as well.

Nevertheless, an improvement that is only applicable to this method is by increasing the photodiode gain. This is because when the amount of light received by the photodiode is only a quarter, increases the photodiode gain can increase the SNR of the image. When this is applied on either CM or NHRC method, the reconstructed image is not accurate as saturation will occur on the photodiode outputs (Sun *et al.*, 2016). Figure 2.3 shows the schematics diagram of CM and QM.

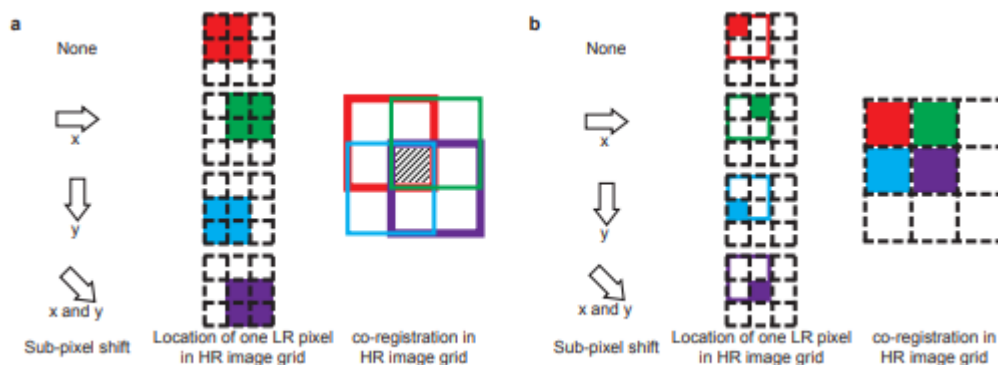


Figure 2.3: Schematics diagram of two digital microscanning method. a) Complete microscanning. b) Quarter microscanning. (Sun *et al.*, 2016)

2.3 Compressed Sensing

Compressed Sensing (CS) is one of the emerging image acquisition techniques in recent years. Conventionally, the entire image is sampled to acquire the data needed for image reconstruction. The redundant information in the data will be further removed when compressed to the required resolution. Meanwhile in CS, only the important information is being sensed by using a series of mask to form a compressed version of image (Dadkhah, Deen and Shirani, 2013). As CS samples only partial of the data, it has a shorter image acquisition time as compared to other techniques.

2.3.1 Basic Framework

Yu *et al.*, (2015) stated that the basic measurement theory of CS can be represented as Equation 2.1:

$$y = \Phi x = \Phi \Psi s = \Theta s \quad (2.1)$$

where

y is the compressed image

x is the original image

Φ is the measurement matrix

Ψ is the orthonormal basis space

Θ is the coding pattern

s is the weighting coefficient vector

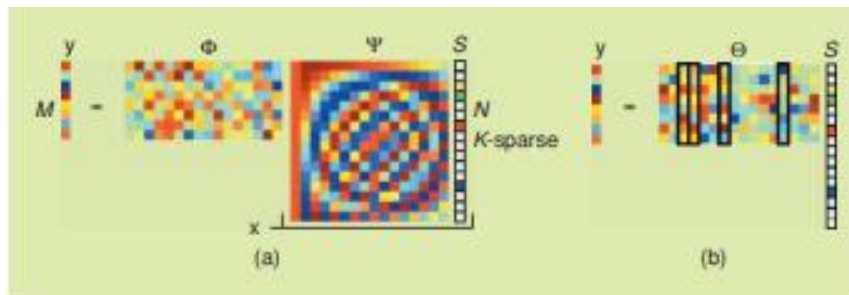


Figure 2.4: Illustration of compressed sensing equation. a) In Φ and Ψ form. b) In Θ form. (Baraniuk, 2007)

Figure 2.4 shows the illustration of CS equation. The image x is transformed into k -sparse of matrix in Ψ domain. The k -sparse represents the sparsity of the data where only meaningful information is presented while the basis Ψ is the image compression technique being used such as discrete cosine transform (DCT), singular value decomposition (SVD), discrete wavelet transform (DWT) and etc. Based on Figure 2.4, the encoding process to get the compressed image is just a simple matrix multiplication. However, the measurement matrix Φ has to be designed properly to get all those vital information. The linear measurement of CS can be expressed as follow:

$$Y_{M \times 1} = \Phi_{M \times N} X_{N \times 1} \quad (2.2)$$

where

M is the total of the measurement performed

N is the total of the pixel.

Only M measurements are acquired instead of all of the pixels which proves the ‘compressed’ theory in CS. Besides, as the M is higher than the order of sparsity k , it complies with the restricted isometry property (RIP) to reconstruct the image (Baraniuk, 2007).

The image can be recovered based on the measurement data obtained. As the matrix satisfies the RIP, the reconstruction process is typically done by using the L1-norm minimization as known as Manhattan norm which can be represented as below:

$$s = \operatorname{argmin} \|s\|_1 \text{ subject to } \Theta s = y \quad (2.3)$$

L1-norm is conventionally used as it has the features of regularization and data fusion which aids in duelling with motion error, outlier, blur and also edge preservation. Other than this, there are a few methods for image reconstruction such as L0-norm, basis pursuit (BP) method and Greedy method but they normally cannot achieve a higher SNR ratio than L1-norm.

2.3.2 Data Acquisition Mechanism

In single pixel imaging, a series of mask projected by DMD is used for data acquisition. Typically, the masks can be formed by various type of measurement matrix such as Pseudorandom and Hadamard matrix. All the masks will have a specific resolution grade only to capture the desire information. Any information that passed through the masks will be captured in the photodiode.

The journal paper “A Portable Single-Pixel Camera Based on Coarse-To-Fine Coding Light” (Yu *et al.*, 2015) had proposed a new image acquisition method called coarse-to-fine model. In this method, an increasing resolution grade of mask is used to grab different outline information of the image. However, the information from the low resolution cannot be directly applied on the reconstruction of image. Thus, a connection between them needs to be formed in order to generate a higher resolution image. So, the image recovery is done by using an adaptive step size pyramid algorithm. It can obtain the distance between each adjacent layer by using the outline

information and image with the same resolution. L1-norm method is then used in every layer to generate the image with the desired resolution. As compared to random matrix and Elad method, this method can achieve a better result in reputation error (RE), structural similarity index measurement (SSIM) and processing time (Yu *et al.*, 2015).

2.4 Image Processing Techniques

The working principle of image processing mainly made up by three phases which is importing the existing data from the image, analysing the image's data and manipulating the data based on the analysis. There are various types of image processing techniques which serve for different functions depend on their mathematical algorithms. Image processing techniques often used to improve the image quality or extract the important information from the image. Within the scope of this project, mainly super resolution and image interpolation are studied to improve the overall quality of the reconstructed image.

2.4.1 Super Resolution

Super resolution (SR) is one of the emerging image processing techniques nowadays. The basic idea of this technique is combining the characteristics of a few low resolution (LR) images to recover a high resolution (HR) image. SR extracts the non-redundant data from the LR images assuming each of them have independent information. SR technique uses the theory of Fourier Transform (FT) and Analytic Continuation (AC) which reconstructed the whole analytic function based on the values in that area (Sudheer Babu and Sreenivasa Murthy, 2011). It aids in extending the domain over a complex analytic function. Let the equation of the imaging model as below:

$$g(x, y) = h(x, y) * f(x, y) + n(x, y) \quad (2.4)$$

where

$g(x, y)$ is the original image

$h(x, y)$ is the reconstructed image

$f(x, y)$ is the domain function

$n(x,y)$ is the noise

Further performing FT on the equation:

$$G(u, v) = H(u, v).F(u, v) + N(u, v) \quad (2.5)$$

SR will use the AC on the $F(u,v)$ to extend its domain in order to construct a higher resolution image, $H(u,v)$. There are two classes of domain representation being used in SR which are the frequency domain class and spatial domain class.

2.4.1.1 Frequency Domain Class

The reconstruction of a HR image is done in the frequency domain before transforming to the spatial domain. Scaria and Yomas, 2014 stated that this SR approach is based on three principles. First is the shifting property of FT, where the image is shifted by translation. Next, the aliasing relationship between the discrete Fourier Transform (DFT) and the continuous Fourier Transform (CFT). The DFT coefficients of the image are aliased to the sample of the CFT of the unknown scene (Sudheer Babu and Sreenivasa Murthy, 2011). Figure 2.5 shows the aliasing of the signals.

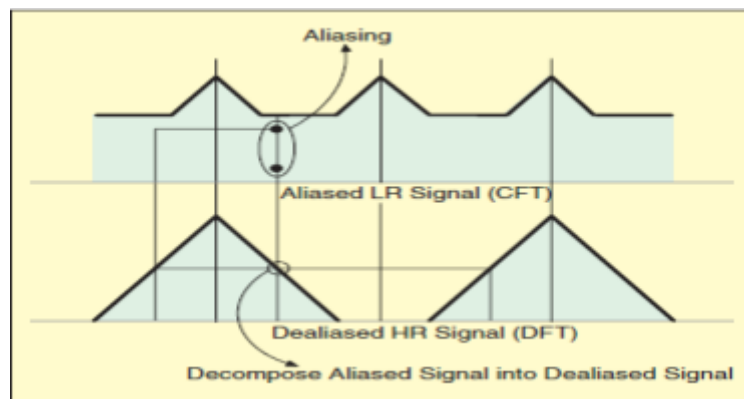


Figure 2.5: Aliasing relationship between DFT and CFT (Makwana and Mehta, 2013).

Last, by assuming the original image is band limited, the aliased equation can be written as:

$$Y = \Phi F \quad (2.6)$$

where

Y is DFT coefficient of the image

Φ is the aliased relationship

F is the domain function.

The frequency domain SR will then determine the Φ and apply an inverse DFT to obtain the reconstructed image.

This SR approach is way more straightforward due to a lower computational complexity when compared to spatial domain class of SR. However, it has a limitation to the global translation in the shifting of image and also space invariant degradation models (Sudheer Babu and Sreenivasa Murthy, 2011).

2.4.1.2 Example-Based Super Resolution

There is another domain class for image reconstruction which is spatial domain. There is no transforming of signal needed as all the image reconstruction process is done in the spatial domain. This approach can cope with both global and non-global translation, optical and motion blur and many others (Makwana and Mehta, 2013). This class had laid the foundation for many SR methods such as example-based super-resolution.

Due to the classical SR method discussed in Section 2.2.1 can only achieve a small increase of resolution with a factor lesser than 2, a new SR approach had been developed, namely Example-Based Super-Resolution. In this method, the sharpening of missing HR information process is replaced by using data from a database of LR and HR image pair. However, this method may not reconstruct a true HR information as it is using an external source.

The algorithm used in this method is known as learning-based or hallucination algorithm. The relationship between HR and LR is learned by using a Markov network and it is used to choose the most appropriate information from the database. Thus, a proper generalization capability is very

important in this algorithm to get a high accuracy of data (Scaria and Yomas, 2014).

2.4.2 Image interpolation

Image interpolation is a common technique used in digital image process such as image resizing or bayer demosaicing. The basic principle of this technique is that it uses the existing data to estimate the unknown data point in between (Fadnavis, 2014). When an image is resized from a smaller pixel grid to a bigger grid, it is necessary to increase the total number of pixels. Thus, image interpolation serves the purpose of estimating the additional pixels' data based on the existing pixels' data from the original image. There are various types of image interpolation algorithms such as nearest neighbor, bilinear, bicubic, lanczos and many others.

2.4.2.1 Nearest Neighbor Interpolation

Nearest neighbor interpolation assigns the interpolated pixels' data using the nearest existing data. This algorithm is the most simplest and efficient among others as it only duplicate the nearby data without any calculations. However, the resulting image has a poor image quality as it has a discontinuity between two data points. Figure 2.6 shows the result of the nearest neighbor interpolation algorithm.

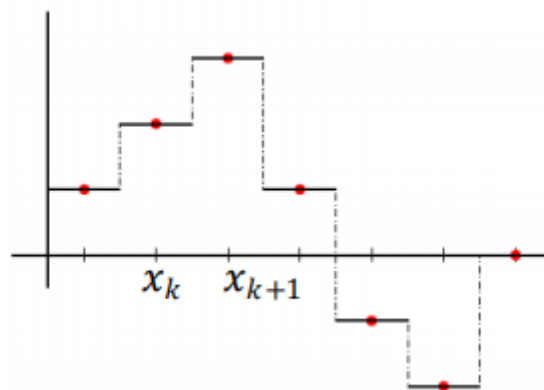


Figure 2.6: Result of the nearest neighbor interpolation algorithm (Howard, 2018).

2.4.2.2 Bilinear Interpolation

Bilinear interpolation assigns the weighted average of four nearby pixels' value to the interpolated pixels' data. The weight is calculated using the distance between source pixel to the targeted pixel. This algorithm will produce a result of lesser distortion as four nearest pixels' data is taken into account (Titus and Geroge, 2013). Figure 2.7 shows the result of the bilinear interpolation algorithm.

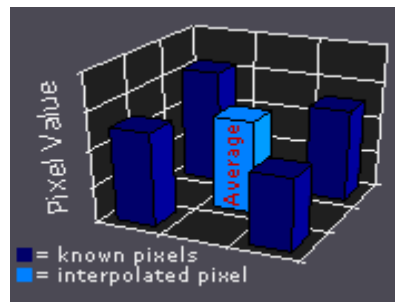


Figure 2.7: Result of the bilinear interpolation algorithm (Understanding Digital Image Interpolation, 2021).

2.4.2.3 Bicubic Interpolation

The only difference between bicubic and bilinear interpolation is that the former one uses 4x4 neighbourhood pixels' data, which is a total of 16 pixel instead of only 4 nearby pixels' data (Titus and Geroge, 2013). As this algorithm involves weighting in calculation, nearer pixels will have a higher weighting. Thus, it provides a lesser distortion result but a greater time is needed for complex calculation. Figure 2.8 shows the result of the bicubic interpolation algorithm.

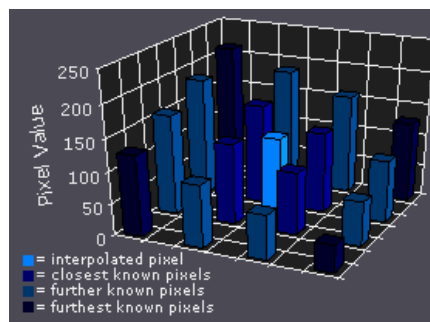


Figure 2.8: Result of the bicubic interpolation algorithm (Understanding Digital Image Interpolation, 2021).

2.4.2.4 Lanczos Interpolation

Lanczos interpolation maps all the pixels' data into a translated and scaled copy of a Lanczos kernel to evaluate the target pixel's data. Lanczos kernel is made up by a sinc function windowed by a central hump of dilated sinc function (Fadnavis, 2014). The total number of nearby pixels for consideration depends on the order of the kernel used in the algorithm such as Lanczos-2, Lanczos-3 and many others. The detail preservation property becomes the main advantage of this technique.

2.5 Summary

Image acquisition and reconstruction are the key components which affect the performance of SPI. Based on the literature review, the Coarse-to-Fine sampling method which can capture different outline information is more suitable for data acquisition in SPI. Besides, implementation of the Super Resolution technique can further improve the image quality. The details of the project will be discussed in Chapter 3.

CHAPTER 3

METHODOLOGY AND WORK PLAN

3.1 Introduction

This project is divided into two parts namely data acquisition which is the front-end process in the SPI framework and image reconstruction which is the back-end part. The flow diagram of SPI framework is illustrated in Figure 3.1.

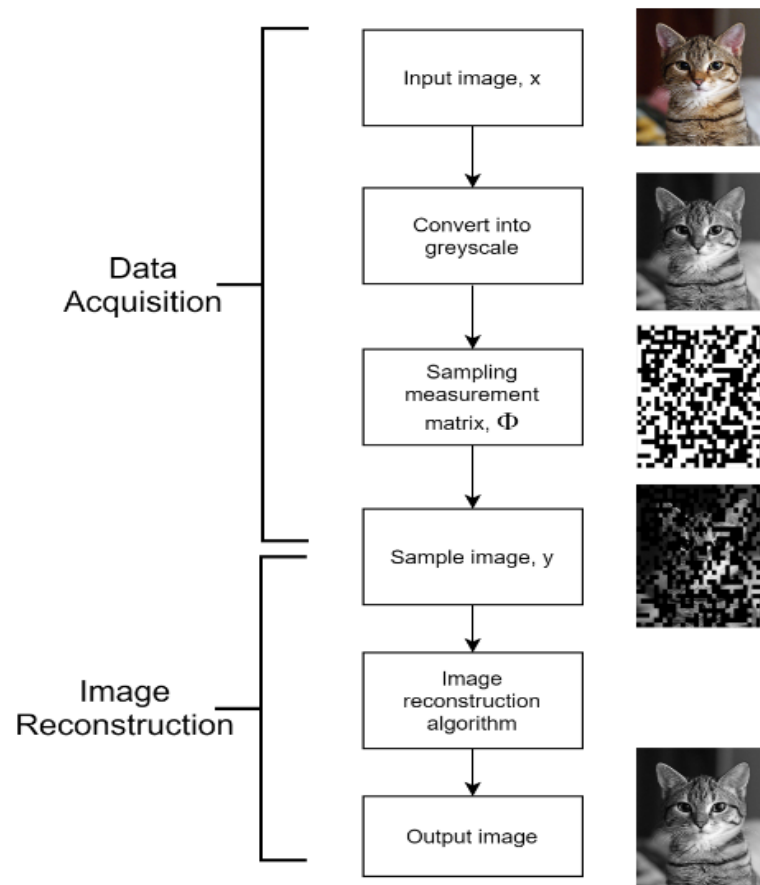


Figure 3.1: Flow diagram of single pixel image processing.

The project planning and problem formulation was done at the beginning of the project. An in-depth literature review and investigation was performed on SPI to establish a background on the project. Next, a preliminary study based on a basic simulation was done to get better insights. The progress of the project for the first semester is shown in Figure 3.2.

No.	Project Activities	Planned Completion Date														
			W1	W2	W3	W4	W5	W6	W7	W8	W9	W10	W11	W12	W13	W14
1.	Project Planning and Problem Formulation	2020-06-26	■	■												
2.	Literature Review and Research Methodology	2020-08-14		■	■	■	■	■	■	■	■					
3.	Investigation into Single Pixel Imaging Technique	2020-08-21					■	■	■	■	■	■				
4.	Perform basic simulation on compressed sensing	2020-09-04										■	■			
5.	Report Writing and Presentation	2020-09-18										■	■	■	■	

Figure 3.2: Gantt chart of the project for first semester.

In the next semester, the model of Coarse-to-Fine sampling method was constructed. Besides, super resolution was implemented in the post-processing phase. Data gathering is done separately for each method. In the last part of this project, the two methods were integrated in a same flow and tested with multiple image dataset. The progress of the project is shown in Figure 3.3.

No.	Project Activities	Planned Completion Date														
			W1	W2	W3	W4	W5	W6	W7	W8	W9	W10	W11	W12	W13	W14
1.	Project Planning	2021-01-24	■	■												
2.	Programming and Debugging	2021-02-26		■	■	■	■	■								
3.	Project Analysis and Data Gathering	2021-03-12						■	■	■						
4.	Code Optimization	2021-03-19							■	■						
5.	Project Testing	2021-03-26								■	■					
6.	Report Writing and Presentation	2021-04-23									■	■	■	■	■	

Figure 3.3: Gantt chart of the project for second semester.

In this project, the CS technique is proposed in the data acquisition to sample the image scene. Meanwhile, the SR algorithm will be implemented to improve the conventional reconstruction algorithm in CS. The combination of these two approaches has the potential to produce a higher image quality.

First, the sampling measurement matrix and the sparse basis are designed to form the ‘mask’ in the DMD. Then, the relationship between the mask with the image scene is studied to determine a most appropriate

reconstruction algorithm. Next, a most effective post-processing technique is designed to implement into the system. All of the steps are performed on simulation platform using Matlab including the testing phase. Lastly, the proposal is validated and analysed for its performance using multiple image datasets. Figure 3.4 shows the overall work plan for this project.

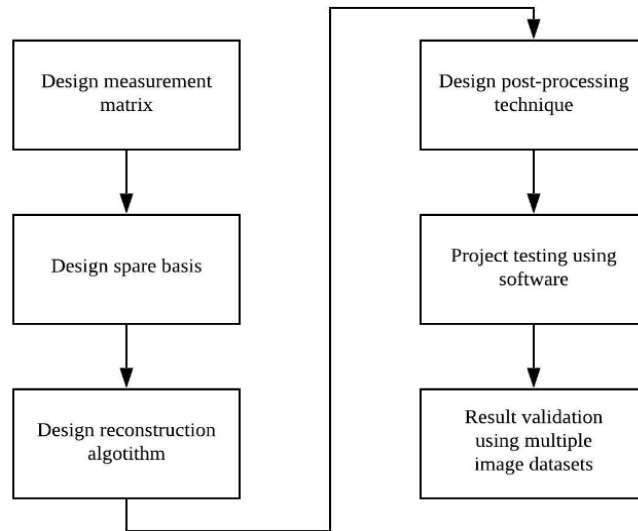


Figure 3.4: Work plan of the project.

3.2 Data Acquisition

In the conventional compressed sensing, a series of DMD masks with a same resolution grade are used for data acquisition in the system. The mask projected by the DMD can be formed by several type of measurement matrix such as Pseudorandom matrix (random) and deterministic matrix (Hadamard). Pseudorandom matrix is a random matrix with value of 1 and 0 while Hadamard matrix is an orthogonal matrix with value of 1 and -1 only. Value 1 denotes for white part while value 0 and -1 denote for black part in the mask. Any information from image that pass through the white part of the mask will be captured in the single pixel detector for later image reconstruction purpose.



Figure 3.5: Sample of masks with a same resolution grade used for data acquisition.

Although this data sampling method is able to capture some of the information from the image, but the reconstructed image based on the limited information cannot achieve a high image quality. This poor performance occurs regardless of the type of masks used in the system. Thus, Hadamard and Pseudorandom mask is both tested to further prove this statement. In this project, images are reconstructed using both type of masks with a same resolution grade of 64×64 . The number of measurements made was set at 3000 which is around 73% of full sampling ratio.

3.2.1 Coarse-to-Fine Sampling Method

To overcome the limitation face in the data acquisition part, a Coarse-to-Fine sampling method is proposed to replace the conventional sampling method. The ‘coarse’ means a low resolution grade of mask while the ‘fine’ means a high resolution grade of mask. So, the mask will start at a low resolution grade and slowly increase until it reached the target resolution. The low resolution grade of mask will responsible for capturing the outline information of the image while the mask with higher resolution will capture the detail information of the image.



Figure 3.6: Sample of masks with an increasing resolution grade (from left to right).

In order to evaluate the performance of this method, same setting as for the conventional method in Section 3.2 is applied to this method. The output image is reconstructed using maximum resolution (finest) of mask at 64×64 and 3000 of measurement is made. The only difference is that this method will not only use a series of 64×64 masks but an increasing resolution grade of mask. Before applying this method, there are several factors that will affect the performance of this Coarse-to-Fine method such as the step size and the minimum resolution (coarsest) to start with.

In this project, the method is tested using 4 step sizes i.e. 1, 2, 4 and 8. The number of measurements made at every resolution grade of mask is carried out evenly. For example, provided that the setting of the method is to start at a minimum resolution at 32×32 with a step size of 8 and 3000 of measurement. Resolution grade for the series of masks used will be at 32, 40, 48, 56 and 64. Along with that, 600 measurements will be made at each layers with a total up of 3000 measurements. The performance for each step size will be evaluate and the best result is taken to compare with the conventional method in Section 3.2.

3.3 Image Post-processing Technique

The reconstructed image has a relatively smaller size than the reference image. Thus, the reconstructed image has to be resized in order to test for its image quality. In this project, image interpolation and super resolution was chosen as the image post-processing technique.

3.3.1 Image interpolation

Various type of image interpolation methods was used to resize the reconstructed image; nearest, bilinear, bicubic, lanczos-2 and lanczos-3 interpolation. Each method have their own algorithm in image processing and their performance is tested with multiple image dataset.

3.3.2 Very Deep Super Resolution

Although interpolation method is very simple to be apply, but it is very difficult to recover a high frequency information from a low resolution image. Therefore, a super resolution method named Very Deep Super Resolution

(VDSR) was proposed to be implemented in the post processing part of the system. This method has a neural network to learn the mapping between low resolution and high resolution image by using deep learning approach. Residual image, which is the difference between a high resolution and low resolution image is determine from the luminance of the image.



Figure 3.7: a) High resolution image. b) Low resolution image. c) Residual image.

The IAPR TC-12 Benchmark which consist of 20000 high resolution images is used as training dataset. All of the images are downsized and resized back to the original size to get a lower resolution of images. Then, all of the low resolution images are compare to their high resolution image respectively to get the residual images. The VDSR network is trained by using the 20000 pair of high resolution images and residual images. Moreover, scale factor of 2, 3 and 4 for image resizing is taken into account so that the VDSR network can cope with a wider range of input image sizes.

Thus, VDSR network can now predicts the residual image and add it into the upsize low resolution image to achieve a higher image quality. It is believed to be perfectly suit into the image processing scheme of single pixel imaging. In this project, VDSR and five type of interpolation methods as stated in Section 3.4 were implemented as the post-processing technique in the system. The performance in terms of image quality and practicability of all of the methods are tested using the reconstructed images from both Hadamard and Pseudorandom masks.

3.4 Proposed Integration of Image Acquisition and Post-processing Scheme

In the previous sections, the performance of both proposed methods (Coarse-to-Fine sampling and Super Resolution) were assessed separately. It is possible to integrate both techniques in the same flow where Coarse-to-Fine sampling is used in data acquisition and VDSR is implemented as the back-end processing of the system. Theoretically, there is no contradiction between these two techniques. Coarse-to-Fine sampling method is able to capture more information and reconstruct a better quality of image. This will help the VDSR network to predict a more accurate residual image to further improve the final image. The performance of the proposed framework is compared to the conventional compressed sensing, Coarse-to-Fine sampling and VDSR method. Figure 3.8 shows the overall system of the proposed method.

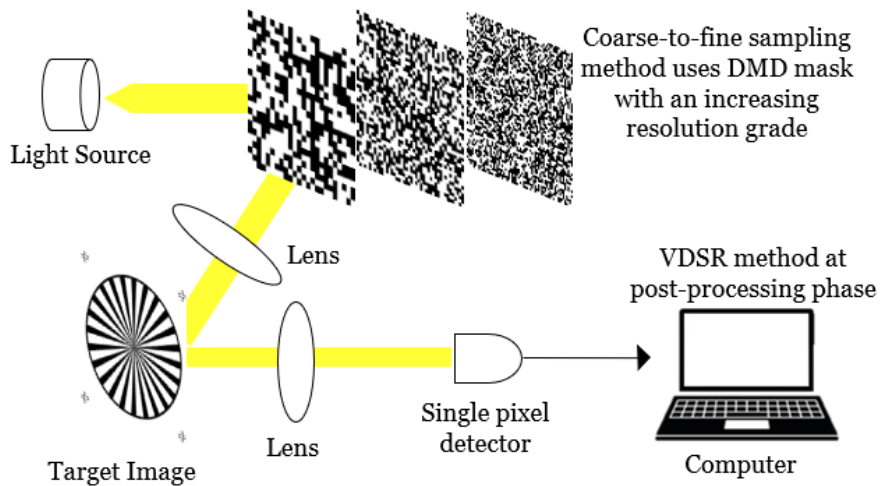


Figure 3.8: Illustration of the proposed system overview.

3.5 Evaluation Methods

Matlab version R2018a is the main software for this project. As it provides many built-in images processing toolbox, it is very suitable to be use to simulate the result. A well-developed library can significantly reduce the time for debugging when carry out the project.

A toolbox named L1magic developed by Justin Romberg is use for solving minimization problem in CS. This toolbox can recover the sparse signal using the convex programming and it provides many types of solutions

each with its advantage and limitation (Abufarag and Vahrenkamp, 1995). Thus, the reconstruction of HR image can be achieved using this toolbox.

Besides, Matlab also provides various types of evaluation methods to measure the quality of the reconstructed image. The methods used in this project are the peak signal-to-noise ratio (PSNR), structural similarity index measurement (SSIM) and root mean square error (RMSE).

3.5.1 Peak Signal-to-Noise Ratio (PSNR)

Peak signal-to-noise ratio (PSNR) is defined as the ratio of the maximum power of a signal to the distorting noise. Usually, an image has a wide dynamic range i.e. a large gap between the maximum and minimum value of in the matrix data. Thus, PSNR is measured using a logarithmic decibel scale, dB. The formula of the PSNR is as follows:

$$PSNR = 20 \log \frac{MAX_f}{\sqrt{MSE}} \quad (3.1)$$

where

MAX_f is the maximum signal value

MSE is the mean square error

The MSE computes the average of the square of the error to the original image. A low level of MSE indicates a better quality of an image. The formula of the MSE is as follows:

$$MSE = \frac{1}{mn} \sum_0^{m-1} \sum_0^{n-1} ||f(i,j) - g(i,j)||^2 \quad (3.2)$$

where

f is the original image

g is the reconstructed image

m is the number of row

n is the number of column

A low value of MSE causes a high PSNR value indicating the noise level is small in the reconstructed image. In shorts, the higher the value of PSNR, the better the quality of the reconstructed.

3.5.2 Structural Similarity Index Measurement (SSIM)

Structural similarity index measurement (SSIM) is defined as the similarity between the original image with the degraded image after image processing such as data compression in this project. Thus, SSIM is a full reference metric as the measurement is made by using the original image as its reference. SSIM also takes into account the perceptual phenomena such as luminance masking and contrast masking. Luminosity masking is the sensitivity of vision to the distortion of different background luminance such as a brighter or darker image area. In addition, the contrast masking is the visibility of an image affected by the presence of similar frequency content or spatial location. When two identical images is compare using SSIM, the result is 1 indicating there are exactly the same. Thus, the nearer the SSIM value to the ideal value of 1, the better the image quality and reconstruction algorithm.

3.5.3 Root Mean Square Error (RMSE)

Root mean square error (RMSE) is defined as the standard deviation of the prediction error which means the concentration of the data at the best fit. In this project, it will be used to measure the amount of change per pixel after an image processing. The formula of the RMSE is as follow:

$$RMSE = \sqrt{\sum_{i=1}^n \frac{(y_i - x_i)^2}{n}} \quad (3.3)$$

where

y is the predicted value

x is the observed value

n is the total measurement

Pradham, Younan and King, 2008 stated that RMSE has a higher resolution compared to the correlation coefficient when comparing the image quality of a

similar reconstruction algorithm. In a nutshell, a lower value of RMSE indicates a better quality of image and also a better image reconstruction algorithm.

3.5.4 Statistical Test

In the data acquisition, Pseudorandom and Hadamard matrix were used as the measurement matrix. Theoretically, Hadamard matrix gives consistent result as it is a deterministic matrix. Thus, the improvement shown by Coarse-to-Fine sampling method with Hadamard mask is a promising proof. On the other hand, Pseudorandom matrix is purely random and result may vary every time. The mask is formed randomly and different information is captured resulting in a different image being reconstructed. Therefore, it is necessary to perform a statistical test to prove that the improvement of the method is not because of sampling error or by chance.

Student's T-Test is chosen as the statistical test in this project. Simulation is run 5 times for every test image to get a variation in data. The P-value is calculated based on the data to prove for significant difference where P-value measures the probability against the null hypothesis of the test.

CHAPTER 4

RESULTS AND DISCUSSION

4.1 Data Acquisition Phase

To assess the performance of the proposed Coarse-to-Fine sampling method, some tests were run and analyzed in order to pre-configure the step size and the lowest resolution grade (coarsest). The result showed that to reconstruct a 64 x 64 resolution of image, the best step size is 4 while the minimum resolution for the mask is 32 x 32. Thus, the resolution of the masks used for the method were 32, 36, 40, 44, 48, 52, 56, 60 and 64. This setting was applied for all the subsequent simulation of Coarse-to-Fine sampling method to ensure a consistent and fair comparison. The configuration for the simulation is as follow:

- Number of measurements: 3000
- Minimum resolution: 32
- Maximum resolution: 64
- Step size: 4

4.1.1 Hadamard Mask

Table 4.1: Quantitative comparison between the normal compressed sensing and Coarse-to-Fine (c2f) sampling method using Hadamard mask. Highlighted results indicate the best performance.

Res 64 Nsamp 3000	PSNR		SSIM		RMSE	
	Normal	c2f	Normal	c2f	Normal	c2f
testpat	10.3318	12.0432	0.4603	0.4666	0.1953	0.1698
blobs	11.5278	14.2982	0.1441	0.1953	0.2336	0.1007
chips	23.6458	24.8393	0.7462	0.7725	0.0457	0.0456
cameraman	18.5563	17.8299	0.6245	0.6607	0.0939	0.1384
foosball	18.5856	18.5296	0.6305	0.6551	0.0692	0.076
cat	17.841	22.3273	0.5721	0.6167	0.1074	0.0592
park	14.4193	16.9385	0.5136	0.5493	0.1791	0.1493
wagon	17.9031	20.9505	0.4601	0.5022	0.1037	0.0427
peacock	17.0462	17.8231	0.3612	0.3687	0.0841	0.0847
sevilla	15.7851	17.8484	0.3481	0.3846	0.1091	0.0861

Table 4.1 shows the comparison of performance between normal compressed sensing and the proposed Coarse-to-Fine sampling method using Hadamard mask. Both method were tested with 10 images with different complexity. We can see that generally the proposed method yields better result especially in term of SSIM. There is a significant increase in PSNR value for most of the reconstructed image except for the image ‘cameraman’ and ‘foosball’. However, an increase in PSNR and SSIM value did not indicate that there will be a positive result in RMSE too. For example, the result from image ‘peacock’. This is because RMSE evaluates the difference in all pixels correspond to the original image while PSNR and SSIM test for the present of noise and the similarity in the image structure respectively. Based on the analysis, the proposed method works well on recovering the structure of the image. Implementing an increasing resolution grade of masks to capture different outline information from the image results in a better SSIM value as compared to the conventional compressed sensing method. Overall, the proposed method achieved better image quality than the conventional method using Hadamard mask.

4.1.2 Pseudorandom Mask

Table 4.2: Quantitative comparison between normal compressed sensing and Coarse-to-Fine (c2f) sampling method using Pseudorandom mask. Highlighted results indicate the best performance.

Res 64	PSNR		SSIM		RMSE	
	Normal	c2f	Normal	c2f	Normal	c2f
testpat	10.671	12.0259	0.4482	0.4608	0.244	0.1603
blobs	13.1986	14.1841	0.1691	0.188	0.1496	0.0971
chips	25.2743	25.2252	0.7484	0.7605	0.0386	0.0424
cameraman	17.748	18.4318	0.6143	0.6461	0.1368	0.123
foosball	18.049	18.5107	0.6265	0.6458	0.0851	0.0717
cat	21.9392	22.2942	0.5825	0.6069	0.0627	0.0629
park	15.4844	16.5039	0.5282	0.5477	0.187	0.1587
wagon	20.6735	20.6879	0.4882	0.4923	0.0529	0.0325
peacock	17.5752	17.6345	0.3587	0.3635	0.0871	0.0879
sevilla	17.4342	17.5137	0.3707	0.385	0.0902	0.0969

Table 4.2 shows the comparison of performance between normal compressed sensing and the proposed Coarse-to-Fine sampling method using Pseudorandom mask. Both methods were tested with the same images in Section 4.1. Most of the best results shown from the proposed Coarse-to-Fine method especially in term of SSIM. From Table 4.2, we can see that there is only a minor increase in PSNR value. Besides that, the change from using Hadamard mask to Pseudorandom mask indicates that the result varies per simulation. A Student T-Test was carried out to further prove the performance of the proposed method on Pseudorandom mask. As discussed in Section 3.5.4, all the simulation were repeated 5 times to collect data for the Student T-Test. The simulated data is shown in Appendix 1. All results in PSNR, SSIM and RMSE were tested. The results in Appendix 2, 3 and 4 show that all of them has a P-value lesser than the significance level of 0.05. This proves that the null hypothesis, H_0 of the Student T-Test is rejected which mean there is a significance difference between the proposed method and the conventional method. Thus, the performance improvement shown in the proposed method is not by chance or due to sampling error during the process.

4.1.3 Discussion

The proposed Coarse-to-Fine sampling method works for both Hadamard and Pseudorandom mask. It successfully achieved positive result in most of the test images. However, the performance varies depends on the content of the image. Thus, it is crucial to improve the proposed method to achieve a consistant image quality.

4.2 Post-processing Phase

The performance of all the post-processing techniques were tested with the reconstructed image from both Hadamard and Pseudorandom mask. The results were tabulated in Table 4.3 and Table 4.4 respectively.

Table 4.3: Quantitative comparison between different interpolation methods and super resolution using the reconstructed images from Hadamard mask.

Highlighted results indicate the best performance.

Res 64 Nsamp 3000	PSNR					
	Interpolation					Super Resolution
	Nearest	Bicubic	Bilinear	Lanczos-2	Lanczos-3	
testpat	10.3318	10.5617	10.1986	10.5667	10.7035	11.1659
blobs	11.5278	11.6017	11.3291	11.6042	11.7101	12.1936
chips	23.6458	24.5918	24.3617	24.598	24.6813	25.2585
cameraman	18.5563	18.9014	18.717	18.905	18.9473	19.2205
foosball	18.5856	19.1424	18.8498	19.1455	19.2233	19.7859
cat	17.841	18.051	17.9072	18.0535	18.0995	18.2419
park	14.4193	14.4968	14.4846	14.4967	14.4943	14.4994
wagon	17.9031	18.0892	17.9492	18.0905	18.1268	18.2934
peacock	17.0462	17.2387	17.2819	17.2376	17.2061	17.0328
sevilla	15.7851	15.9317	15.8003	15.9316	15.9619	16.0484

Res 64 Nsamp 3000	SSIM					
	Interpolation					Super Resolution
	Nearest	Bicubic	Bilinear	Lanczos-2	Lanczos-3	
testpat	0.4603	0.4924	0.4688	0.4917	0.4972	0.561
blobs	0.1441	0.1431	0.1227	0.1432	0.15	0.1986
chips	0.7462	0.8037	0.7965	0.8029	0.8031	0.832
cameraman	0.6245	0.6485	0.6375	0.6483	0.6479	0.6738
foosball	0.6305	0.6869	0.6777	0.6859	0.6832	0.7149
cat	0.5721	0.6133	0.5946	0.6136	0.6189	0.6386
park	0.5136	0.5479	0.5386	0.5475	0.5461	0.5576
wagon	0.4601	0.4924	0.4753	0.4925	0.4951	0.5201
peacock	0.3612	0.3882	0.3669	0.3884	0.3917	0.4028
sevilla	0.3481	0.3604	0.3376	0.3602	0.3652	0.3975

Res 64 Nsamp 3000	RMSE					
	Interpolation					Super Resolution
	Nearest	Bicubic	Bilinear	Lanczos-2	Lanczos-3	
testpat	0.1953	0.1961	0.1975	0.1962	0.1964	0.1958
blobs	0.2336	0.2332	0.2331	0.2332	0.2333	0.2333
chips	0.0457	0.0434	0.0429	0.0434	0.0436	0.0426
cameraman	0.0939	0.0935	0.0931	0.0936	0.0937	0.0943
foosball	0.0692	0.0676	0.0666	0.0676	0.068	0.0692
cat	0.1074	0.1042	0.1059	0.1041	0.104	0.0999
park	0.1791	0.1792	0.1792	0.1792	0.1792	0.1797
wagon	0.1037	0.1029	0.102	0.1029	0.1033	0.1041
peacock	0.0841	0.0813	0.08	0.0814	0.0824	0.0868
sevilla	0.1091	0.1052	0.1046	0.1051	0.1055	0.1062

Table 4.4: Quantitative comparison between different interpolation methods and super resolution using the reconstructed images from Pseudorandom mask. Highlighted results indicate the best performance.

Res 64 Nsamp 3000	PSNR					
	Interpolation					Super Resolution
	Nearest	Bicubic	Bilinear	Lanczos-2	Lanczos-3	
testpat	11.6291	12.0802	11.5319	12.0876	12.2903	12.9933
blobs	13.3326	13.6078	13.131	13.6112	13.7914	14.791
chips	24.8127	26.1513	25.8588	26.1594	26.2802	27.0585
cameraman	17.9066	18.238	18.1025	18.2411	18.275	18.5195
foosball	18.3792	18.8855	18.5972	18.8886	18.976	19.5555
cat	22.0309	22.6323	22.1985	22.6398	22.7865	23.18
park	16.8729	17.0275	17.0273	17.027	17.0179	17.0191
wagon	20.5649	20.9921	20.7362	20.9942	21.0577	21.3625
peacock	17.9512	18.1988	18.2552	18.1976	18.1606	17.9768
sevilla	17.463	17.7722	17.6034	17.7714	17.8028	17.8932

Res 64 Nsamp 3000	SSIM					
	Interpolation					Super Resolution
	Nearest	Bicubic	Bilinear	Lanczos-2	Lanczos-3	
testpat	0.4652	0.521	0.5011	0.52	0.5229	0.5746
blobs	0.1701	0.1768	0.1555	0.177	0.1842	0.2393
chips	0.7519	0.8118	0.8051	0.8109	0.811	0.8308
cameraman	0.6199	0.6602	0.6546	0.6598	0.6559	0.6624
foosball	0.6309	0.6969	0.69	0.6959	0.6927	0.7066
cat	0.5928	0.6457	0.6327	0.6457	0.6484	0.6466
park	0.533	0.5748	0.5673	0.5744	0.5719	0.5754
wagon	0.4856	0.5252	0.5083	0.5251	0.5266	0.5449
peacock	0.3655	0.3956	0.3759	0.3957	0.3987	0.4069
sevilla	0.3709	0.3941	0.3729	0.3938	0.3973	0.4187

Res 64 Nsamp 3000	RMSE					
	Interpolation					Super Resolution
	Nearest	Bicubic	Bilinear	Lanczos-2	Lanczos-3	
testpat	0.1906	0.1909	0.1929	0.1911	0.1911	0.1898
blobs	0.136	0.135	0.1346	0.135	0.1354	0.1365
chips	0.0438	0.0412	0.041	0.0413	0.0413	0.0404
cameraman	0.137	0.1369	0.1367	0.1369	0.1371	0.1374
foosball	0.0818	0.0806	0.0801	0.0806	0.0808	0.0824
cat	0.0618	0.0565	0.0595	0.0564	0.0556	0.0456
park	0.1573	0.1571	0.157	0.1571	0.1572	0.1577
wagon	0.0416	0.0375	0.0377	0.0375	0.0375	0.0402
peacock	0.0807	0.0777	0.076	0.0778	0.0789	0.0825
sevilla	0.0937	0.0887	0.0883	0.0887	0.0891	0.091

Based on Table 4.3 and 4.4, the VDSR dominates all the interpolation methods in term of PSNR and SSIM. However, bilinear interpolation yields a better result than VDSR in term of RMSE. This is because VDSR make use of deep learning approach to estimate the possible information to add into the final image when resizing. Thus, the SSIM of the final image will be higher and it is proven based on the data obtained. Besides, as VDSR network is

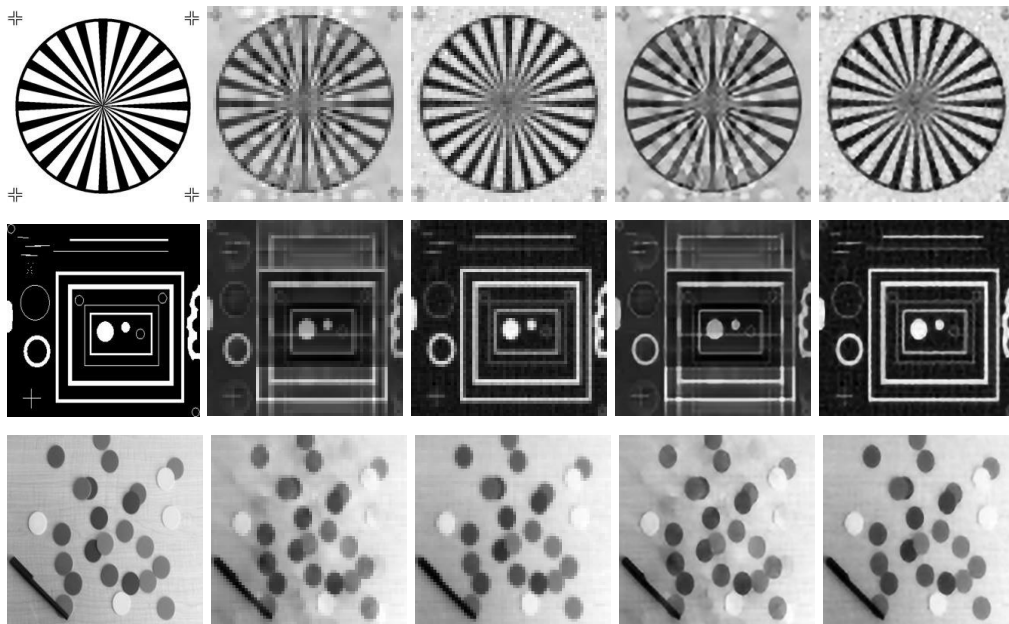
trained using various scale factor of residual image, the resize image will have a relatively low noise level as compared to other methods. On the other side, the algorithm of the bilinear interpolation is to calculate the missing pixels' data based on the neighbour data and their weighting. It maybe not reliable for all images because the neighbour data maybe totally not relatable to the missing pixel's data and resulting in a rogue data.

In short, VDSR technique is the most suitable to implement as the post-processing technique in the processing scheme as it outperformed other methods. Although this technique has its flaw in improving SSIM of the result, but it can be improve by providing more image dataset for its network to train so that it can predict a more accurate residual image in the future.

4.3 Proposed Integration of Image Acquisition and Post-processing Scheme

Results in Section 4.1 and 4.2 showed that Coarse-to-Fine sampling method and VDSR achieved the best performance in data acquisition and post-processing phase respectively. Therefore, two methods were proposed to integrate in a same flow to further improve the overall result. The proposed integration method was tested using both Hadamard and Pseudorandom mask.

4.3.1 Hadamard Mask



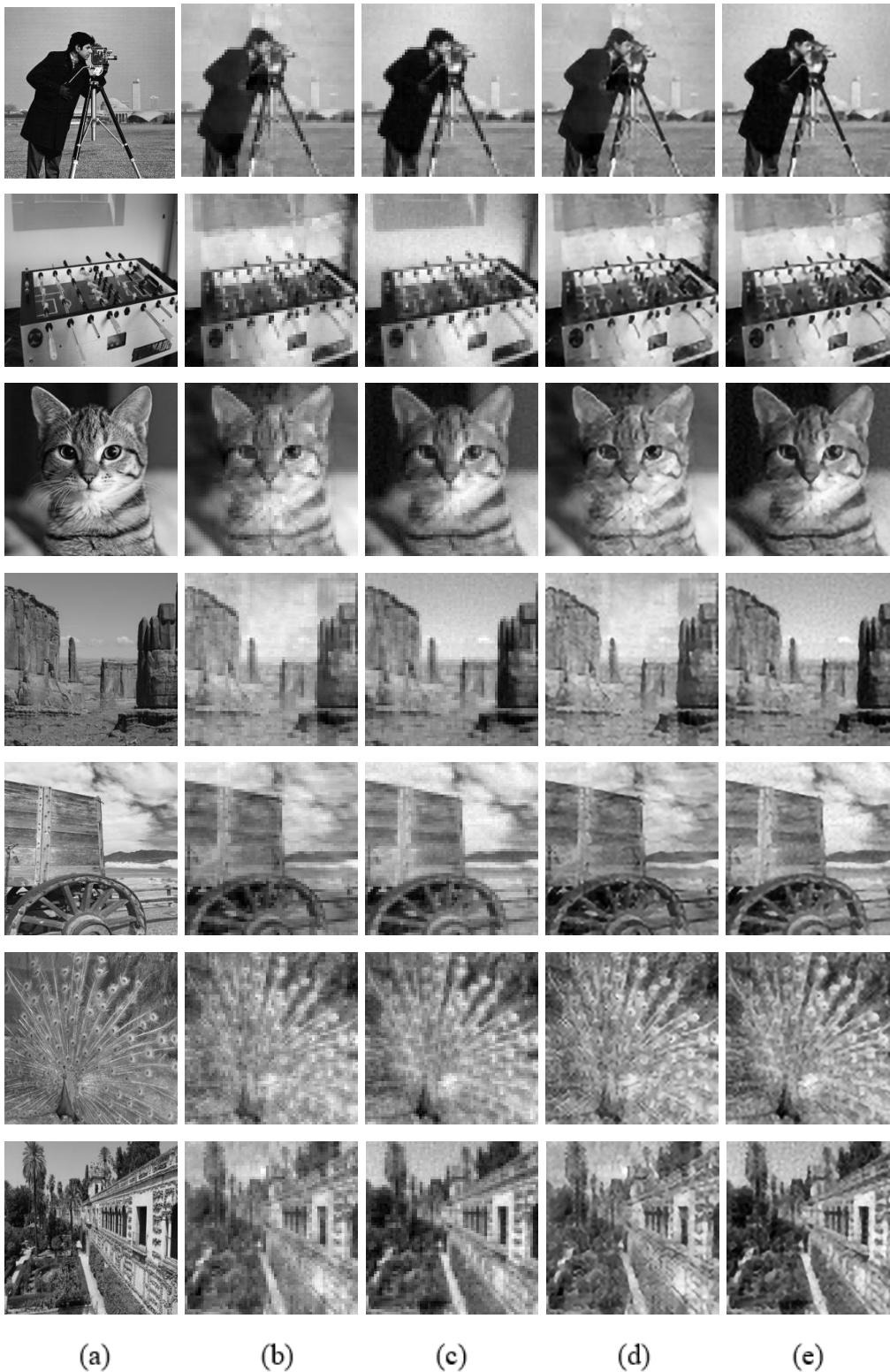


Figure 4.1: Qualitative comparison between different method implemented using Hadamard masks. a) Ground truth, b) Conventional compressed sensing, c) Coarse-to- Fine sampling method only, d) Very Deep Super Resolution (VDSR) only, and e) Proposed integration method.

Table 4.5: Quantitative comparison between different method implemented using Hadamard masks. A) Conventional compressed sensing, B) Coarse-to-Fine sampling method, C) Very Deep Super Resolution (VDSR), and D) Proposed integration method. Highlighted results indicate the best performance.

Res 64 Nsamp 3000	PSNR			
	A	B	C	D
testpat	10.3318	12.0432	11.1659	13.6299
blobs	11.5278	14.2982	12.1936	16.5611
chips	23.6458	24.8393	25.2585	27.2895
cameraman	18.5563	17.8299	19.2205	18.4676
foosball	18.5856	18.5296	19.7859	19.8223
cat	17.841	22.3273	18.2419	23.6548
park	14.4193	16.9385	14.4994	17.0958
wagon	17.9031	20.9505	18.2934	21.9454
peacock	17.0462	17.8231	17.0328	17.8526
sevilla	15.7851	14.8484	16.0484	18.386

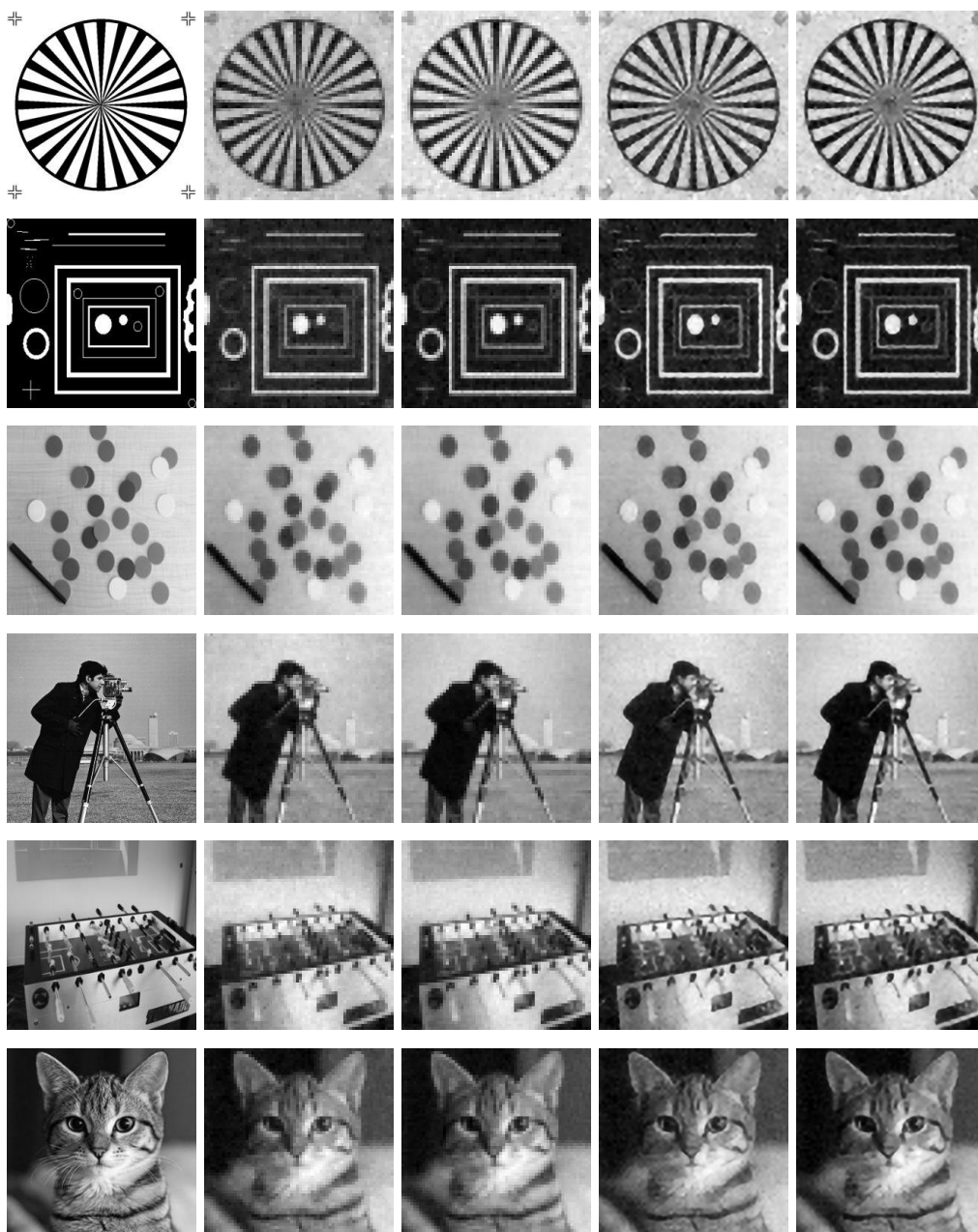
Res 64 Nsamp 3000	SSIM			
	A	B	C	D
testpat	0.4603	0.4666	0.561	0.5887
blobs	0.1441	0.1953	0.1986	0.2805
chips	0.7462	0.7725	0.832	0.8616
cameraman	0.6245	0.6607	0.6738	0.7168
foosball	0.6305	0.6551	0.7149	0.7415
cat	0.5721	0.6167	0.6386	0.6791
park	0.5136	0.5493	0.5576	0.5937
wagon	0.4601	0.5022	0.5201	0.5715
peacock	0.3612	0.3687	0.4028	0.4123
sevilla	0.3481	0.3846	0.3975	0.438

Res 64 Nsamp 3000	RMSE			
	A	B	C	D
testpat	0.1953	0.1698	0.1958	0.1703
blobs	0.2336	0.1007	0.2333	0.1001
chips	0.0457	0.0456	0.0426	0.0422
cameraman	0.0939	0.1384	0.0943	0.1385
foosball	0.0692	0.076	0.0692	0.0763
cat	0.1074	0.0592	0.0999	0.0447
park	0.1791	0.1493	0.1797	0.1498
wagon	0.1037	0.0427	0.1041	0.0403
peacock	0.0841	0.0847	0.0868	0.0856
sevilla	0.1091	0.0861	0.1062	0.0823

Figure 4.1 and Table 4.5 show all the images and data obtained throughout the project using Hadamard mask. There are total four kind of methods i.e. conventional compressed sensing, Coarse-to-Fine sampling method, VDSR and integration method. Among all the methods, we can see that the

integration method yields the best result especially in term of SSIM. On the other side, improvement in RMSE is the biggest drawback for the integration method as it only achieved five best RMSE results among ten test images. In addition, conventional compressed sensing obtained the best RMSE result for image ‘cameraman’. All of the proposed approaches did not work well for this image to improve the RMSE value. All the proposed methods are not perfect enough to ensure a certain improvement for every images.

4.3.2 Pseudorandom Mask



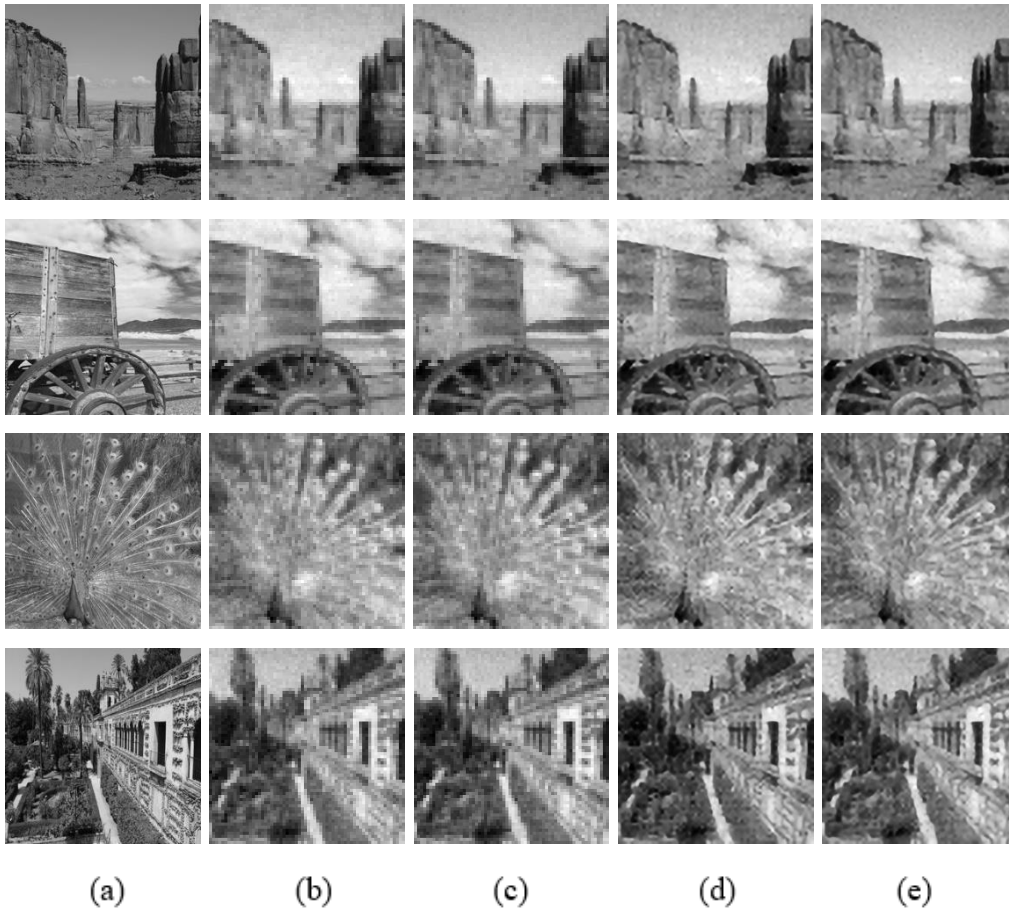


Figure 4.2: Qualitative comparison between different method implemented using Pseudorandom masks. a) Ground truth, b) Conventional compressed sensing, c) Coarse-to- Fine sampling method only, d) Very Deep Super Resolution (VDSR) only, and e) Proposed integration method.

Table 4.6: Quantitative comparison between different method implemented using Pseudorandom masks. A) Conventional compressed sensing, B) Coarse-to- Fine sampling method only, C) Very Deep Super Resolution (VDSR) only, and D) Proposed integration method. Highlighted results indicate the best performance.

Res 64 Nsamp 3000	PSNR			
	A	B	C	D
testpat	10.671	12.0259	12.9933	13.3788
blobs	13.1986	14.1841	14.791	16.0241
chips	25.2743	25.2252	27.0585	27.989
cameraman	17.748	18.4318	18.5195	17.2854
foosball	18.049	18.5107	19.5555	20.3141
cat	21.9392	22.2942	23.18	23.5637
park	15.4844	16.5039	17.0191	17.05
wagon	20.6735	20.6879	21.3625	21.822
peacock	17.5752	17.6345	17.9768	18.4923
sevilla	17.4342	17.5137	17.8932	17.8539

Res 64 Nsamp 3000	SSIM			
	A	B	C	D
testpat	0.4482	0.4608	0.5746	0.5923
blobs	0.1691	0.188	0.2393	0.2618
chips	0.7484	0.7605	0.8308	0.8455
cameraman	0.6143	0.6461	0.6624	0.6899
foosball	0.6265	0.6458	0.7066	0.7203
cat	0.5825	0.6069	0.6466	0.6576
park	0.5282	0.5477	0.5754	0.5941
wagon	0.4882	0.4923	0.5449	0.5692
peacock	0.3587	0.3635	0.4069	0.4115
sevilla	0.3707	0.385	0.4187	0.4274

Res 64 Nsamp 3000	RMSE			
	A	B	C	D
testpat	0.244	0.1603	0.1898	0.1712
blobs	0.1496	0.0971	0.1365	0.1067
chips	0.0386	0.0424	0.0404	0.0363
cameraman	0.1368	0.123	0.1374	0.1662
foosball	0.0851	0.0717	0.0824	0.065
cat	0.0627	0.0629	0.0456	0.0503
park	0.187	0.1587	0.1577	0.1497
wagon	0.0529	0.0325	0.0402	0.0425
peacock	0.0871	0.0879	0.0825	0.0821
sevilla	0.0902	0.0969	0.091	0.0897

Figure 4.2 and Table 4.6 showed all the images and data obtained throughout the project using Pseudorandom mask. There are total four kind of methods; conventional compressed sensing, Coarse-to-Fine sampling method, VDSR and integration method. We can see that the integration method achieved the

best result among others even the masks used are replaced with Pseudorandom mask. However, the integration method only obtained five best RMSE among 10 test images which is same with Hadamard mask. Besides, none of the best result shown from the conventional compressed sensing method. Overall, all the proposed approaches achieved a certain improvement in image quality and is perfectly suit for the system with Pseudorandom mask.

4.3.3 Discussion

Throughout the project, we can say that the integration method is the best image processing scheme for single pixel imaging as it yields the best results among other methods. Theoretically, different outline information is captured in the data acquisition resulting in a high quality of image being reconstructed. An image with better content helps the VDSR network to predict a more accurate residual image. Thus, it will achieve a better image quality in term of PSNR, SSIM and RMSE. Besides, the integration method also works well for both Hadamard and Pseudorandom mask. The integration method has a high efficiency and practicability where it does not depend on the mask used. However, there are still a lot of improvements can be done to further improve the method.

CHAPTER 5

CONCLUSION AND RECOMMENDATION

5.1 Conclusion

This project has improved the performance of single pixel imaging (SPI) through image processing technique. The commonly used data acquisition and image post-processing techniques are not sufficient to produce a high-quality image. The conventional sampling method is replaced by Coarse-to-Fine sampling method. This approaches has successfully captured different outline information for image reconstruction results a better image quality. Besides, Very Deep Super Resolution (VDSR) further enhanced the quality of the final image by estimating the possible residual image based on the pretrained network. Integration of both technique on the processing scheme results in a great improvement on the performance of SPI especially in term of Structural Similarity Index Measurement (SSIM). The simulation in this project were limited in a small sample size but in a number that is adequate for this study.

5.2 Recommendation for Future Work

The step size of the proposed Coarse-to-Fine sampling method in this project is determined based on the test images used. A fixed step size may yield a different result in different images. It would be interesting to figure out an algorithm to determine the best step size for different images.

Besides, the improvement in RMSE still remain the drawback of the processing scheme. To address this problem, the VDSR network to predict the residual image should be improved by providing pair of image datasets with a low RMSE difference in future.

REFERENCES

- Abufarag, A. and Vahrenkamp, H., 1995. Additions and Corrections: A Tripod Ligand with Three Different “Legs” and Some Chiral Zinc Complexes Thereof (Inorganic Chemistry (1995) 34(12) (3279–3284) (10.1021/ic00116a021)), *Inorganic Chemistry*, 34(19), p. 4930. <http://dx.doi.org/10.1021/ic00123a032>.
- AXIS, 2010. CCD and CMOS sensor technology Technical white paper Table of contents, *Axis Communications*, pp. 1–8.
- Baraniuk, R. G., 2007. Compressive Sensing, (July), pp. 2007–2010.
- Baraniuk, R. G. *et al.*, 2011. An introduction to compressive sensing. Available at: <<http://cnx.org/content/col11133/latest>> [Accessed 7 July 2020].
- Cambridgeincolour.com., 2021. Understanding Digital Image Interpolation, [online] Available at: <<https://www.cambridgeincolour.com/tutorials/image-interpolation.htm>> [Accessed 2 April 2021].
- Chippada, U. *et al.*, 2010. Alteration of fibroblast cell behavior due to contraction of substrate, *ASME 2010 Summer Bioengineering Conference, SBC 2010*, (PARTS A AND B), pp. 195–196. <http://dx.doi.org/10.1115/SBC2010-19507>.
- Dadkhah, M., Deen, J. M. and Shirani, S., 2013. Compressive sensing image sensors-hardware implementation, *Sensors (Switzerland)*, 13(4), pp. 4961–4978. <http://dx.doi.org/10.3390/s130404961>.
- Duarte, M. F. *et al.*, 2008. Single-pixel imaging via compressive sampling: Building simpler, smaller, and less-expensive digital cameras, *IEEE Signal Processing Magazine*, 25(2), pp. 83–91. <http://dx.doi.org/10.1109/MSP.2007.914730>.
- Edgar, M. P. *et al.*, 2015. Simultaneous real-time visible and infrared video with single-pixel detectors, *Scientific Reports*. Nature Publishing Group, 5, pp. 1–8. <http://dx.doi.org/10.1038/srep10669>.
- Edgar, M. P., Gibson, G. M. and Padgett, M. J., 2019. Principles and prospects for single-pixel imaging, *Nature Photonics*, 13(1), pp. 13–20. <http://dx.doi.org/10.1038/s41566-018-0300-7>.
- Fadnavis, S., 2014. Image Interpolation Techniques in Digital Image Processing: An Overview, *Journal of Engineering Research and Applications*, 4(10), pp. 70–73. Available at: <www.ijera.com> [Accessed 2 August 2020].
- Howard, J. P., 2018. Interpolation and Extrapolation, *Computational Methods for Numerical Analysis with R*, (February), pp. 95–132. <http://dx.doi.org/10.1201/9781315120195-4>.

Jauregui-Sánchez, Y. *et al.*, 2018. Single-Pixel Imaging Using Photodiodes, *Photodetectors [Working Title]*, (December). <http://dx.doi.org/10.5772/intechopen.79734>.

Kuusela, T. A., 2019. Single-pixel camera, *American Journal of Physics*. American Association of Physics Teachers, 87(10), pp. 846–850. <http://dx.doi.org/10.1119/1.5122745>.

Liu, J. P. *et al.*, 2020. High-quality image retrieval by iterative total-error compensation for single-pixel imaging of random illuminations, *Optics and Lasers in Engineering*. Elsevier Ltd, 124(March 2019). <http://dx.doi.org/10.1016/j.optlaseng.2019.105852>.

Lyu, M. *et al.*, 2017. Deep-learning-based ghost imaging, *Scientific Reports*. Springer US, 7(1), pp. 1–6. <http://dx.doi.org/10.1038/s41598-017-18171-7>.

Makwana, R. R. and Mehta, N. D., 2013. Survey on Single image Super Resolution Techniques, 5(5), pp. 23–33.

Ni.com., 2020. Peak Signal-To-Noise Ratio As An Image Quality Metric. [online] Available at: <<https://www.ni.com/en-my/innovations/white-papers/11/peak-signal-to-noise-ratio-as-an-image-quality-metric.html>> [Accessed 1 September 2020].

Phillips, D. B. *et al.*, 2017. Adaptive foveated single-pixel imaging with dynamic supersampling, *Science Advances*, 3(4), pp. 1–11. <http://dx.doi.org/10.1126/sciadv.1601782>.

Pradham, P., Younan, N. H. and King, R. L., 2008. Concepts of image fusion in remote sensing applications, in *Image Fusion*, pp. 393–428. <http://dx.doi.org/10.1016/b978-0-12-372529-5.00019-6>.

Scaria, R. and Yomas, J., 2014. A Survey of Single Image and Multi Image Super Resolution Techniques, *International Journal of Science and Research*, 3(11), pp. 2012–2015.

Shi, D. *et al.*, 2015. Enhancing resolution of single-pixel imaging system, *Optical Review*. Springer Japan, 22(5), pp. 802–808. <http://dx.doi.org/10.1007/s10043-015-0136-z>.

Sudheer Babu, R. and Sreenivasa Murthy, K. E., 2011. A Survey on the methods of Super-resolution Image Reconstruction, *International Journal of Computer Applications*, 15(2), pp. 1–6. <http://dx.doi.org/10.5120/1923-2568>.

Sun, M.-J. *et al.*, 2016. Improving the signal-to-noise ratio of single-pixel imaging using digital microscanning, *Optics Express*, 24(10), p. 10476. <http://dx.doi.org/10.1364/oe.24.010476>.

Sun, M. J. and Zhang, J. M., 2019. Single-pixel imaging and its application in three-dimensional reconstruction: A brief review, *Sensors (Switzerland)*, 19(3), pp. 1–14. <http://dx.doi.org/10.3390/s19030732>.

Titus, J. and Geroge, S., 2013. A Comparison Study On Different Interpolation Methods Based On Satellite Images, *International Journal of Engineering Research & Technology*, 2(6), pp. 82–85. Available at: <www.ijert.org> [Accessed 6 March 2021].

Yu, H. *et al.*, 2015. A portable single-pixel camera based on coarse-to-fine coding light, *IST 2015 - 2015 IEEE International Conference on Imaging Systems and Techniques, Proceedings*, pp. 1–5. <http://dx.doi.org/10.1109/IST.2015.7294472>.

Zhao, C. H. and Xu, Y. L., 2011. An improved compressed sensing reconstruction algorithm based on artificial neural network, *2011 International Conference on Electronics, Communications and Control, ICECC 2011 - Proceedings*, pp. 1860–1863. <http://dx.doi.org/10.1109/ICECC.2011.6066532>.

APPENDICES

Appendix 1: Data for Student T-Test.

Res 64 Nsamp 3000	PSNR		SSIM		RMSE		Res 64 Nsamp 3000	PSNR		SSIM		RMSE	
	Normal	c2f	Normal	c2f	Normal	c2f		Normal	c2f	Normal	c2f	Normal	c2f
testpat	10.671	12.03	0.4482	0.461	0.244	0.16	cat	21.939	22.29	0.5825	0.607	0.0627	0.063
	11.758	11.94	0.4535	0.465	0.169	0.1734		21.85	22.29	0.596	0.602	0.0613	0.061
	11.514	11.77	0.456	0.4655	0.1931	0.187		21.964	22.24	0.5867	0.597	0.061	0.0625
	11.758	11.8	0.4635	0.466	0.169	0.1737		22.038	22.38	0.5964	0.613	0.0619	0.061
	11.586	11.95	0.455	0.4538	0.1773	0.158		22.053	22.3	0.593	0.603	0.0639	0.062
blobs	13.199	14.18	0.1691	0.188	0.1496	0.097	park	15.484	16.5	0.5282	0.548	0.187	0.159
	13.442	14.11	0.1723	0.184	0.1354	0.102		16.444	18.98	0.5332	0.553	0.1638	0.11
	13.869	13.98	0.182	0.183	0.1125	0.111		16.727	16.91	0.5261	0.549	0.1643	0.153
	13.663	13.89	0.1776	0.18	0.1255	0.116		16.458	16.91	0.5332	0.547	0.1635	0.152
	13.397	13.86	0.1735	0.18	0.1335	0.117		16.238	16.37	0.5345	0.545	0.1695	0.166
chips	25.27	25.225	0.7484	0.761	0.039	0.0424	wagon	20.674	20.69	0.4882	0.492	0.0529	0.033
	25.032	25.6	0.7527	0.762	0.0411	0.035		20.567	20.81	0.4809	0.494	0.042	0.0418
	24.581	24.78	0.7498	0.766	0.0502	0.045		20.542	20.75	0.4859	0.496	0.04	0.0596
	24.95	24.503	0.7461	0.767	0.039	0.0506		20.795	20.81	0.4876	0.498	0.046	0.0553
	24.89	24.604	0.7478	0.767	0.044	0.0495		20.79	20.682	0.4853	0.497	0.0507	0.036
cameraman	17.748	18.43	0.6143	0.646	0.1368	0.123	peacock	17.575	17.63	0.3587	0.364	0.087	0.0879
	17.755	18.44	0.6205	0.648	0.1404	0.122		16.95	16.859	0.3607	0.364	0.091	0.0962
	17.748	18.43	0.6143	0.646	0.1368	0.123		17.628	18.28	0.3594	0.369	0.0849	0.081
	18.78	18.586	0.6231	0.644	0.116	0.1203		18.02	17.335	0.363	0.366	0.083	0.0885
	17.792	18.52	0.6195	0.647	0.1375	0.119		17.497	17.95	0.3589	0.367	0.0879	0.081
foosball	18.049	18.51	0.6265	0.646	0.0851	0.072	sevilla	17.434	17.51	0.3707	0.385	0.09	0.0969
	18.31	18.265	0.6286	0.643	0.0615	0.079		17.241	17.67	0.3646	0.389	0.1043	0.093
	18.049	18.51	0.6265	0.646	0.0851	0.072		17.245	17.58	0.3696	0.379	0.1037	0.093
	18.031	18.34	0.6285	0.642	0.0842	0.078		17.4	17.368	0.3701	0.383	0.094	0.1016
	17.45	18.85	0.6257	0.647	0.096	0.07		17.447	17.68	0.374	0.383	0.094	0.0944

Appendix 2: Result of Student T-Test for PSNR value.

Paired sample T-test, using T distribution (df=49) (two-tailed) (validation)

1. H_0 hypothesis

Since p-value < α , H_0 is rejected.

The average of **After minus Normal's** population is considered to be **not equal** to the μ_0 .

In other words, the difference between the average of **After minus Normal** and the μ_0 is big enough to be statistically significant.

2. P-value

The p-value equals **0.00001033**, ($p(x \leq T) = 1$). It means that the chance of type I error (rejecting a correct H_0) is small: 0.00001033 (0.001%).

The smaller the p-value the more it supports H_1 .

3. The statistics

The test statistic T equals **4.9155**, which is not in the 95% region of acceptance: [-2.0096 ; 2.0096].

$x=0.35$, is not in the 95% region of acceptance: [-0.1438 ; 0.1438].

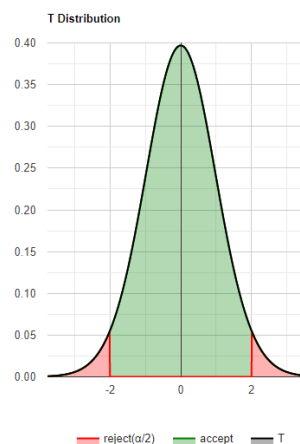
The standard deviation of the difference, S' equals 0.0716, is used to calculate the statistic.

4. Effect size

The observed effect size d is **large, 0.7**. This indicates that the magnitude of the difference between the average and μ_0 is large.

If you like the page, please share or like. Questions, comments and suggestions are appreciated. (statskingdom@gmail.com)

Like 51 Share



Appendix 3: Result of Student T-Test for SSIM value.

Paired sample T-test, using T distribution (df=49) (two-tailed) (validation)

1. H_0 hypothesis

Since $p\text{-value} < \alpha$, H_0 is rejected.

The average of **After minus Normal's** population is considered to be **not equal to** the μ_0 .

In other words, the difference between the average of **After minus Normal** and the μ_0 is big enough to be statistically significant.

2. P-value

The p-value equals **2.22e-16**, ($p(x \leq T) = 1$). It means that the chance of type I error (rejecting a correct H_0) is small: 2.22e-16 (2.2e-14%).

The smaller the p-value the more it supports H_1 .

3. The statistics

The test statistic T equals **12.1328**, which is not in the 95% region of acceptance: [-2.0096 : 2.0096].

$\bar{x} = 0.014$, is not in the 95% region of acceptance: [-0.002251 : 0.002251].

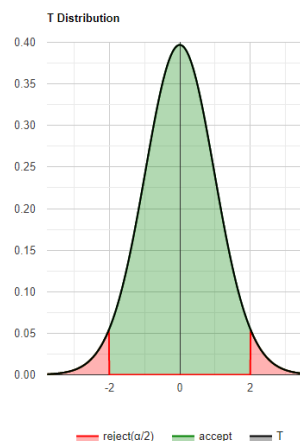
The standard deviation of the difference, S' equals 0.00112, is used to calculate the statistic.

4. Effect size

The observed effect size d is **large, 1.72**. This indicates that the magnitude of the difference between the average and μ_0 is large.

If you like the page, please share or like. Questions, comments and suggestions are appreciated. (statskingdom@gmail.com)

Like 51 Share



Appendix 4: Result of Student T-Test for RMSE value.

Paired sample T-test, using T distribution (df=49) (two-tailed) (validation)

1. H_0 hypothesis

Since $p\text{-value} < \alpha$, H_0 is rejected.

The average of **After minus Normal's** population is considered to be **not equal to** the μ_0 .

In other words, the difference between the average of **After minus Normal** and the μ_0 is big enough to be statistically significant.

2. P-value

The p-value equals **0.0008212**, ($p(x \leq T) = 0.0004106$). It means that the chance of type I error (rejecting a correct H_0) is small: 0.0008212 (0.082%).

The smaller the p-value the more it supports H_1 .

3. The statistics

The test statistic T equals **-3.5659**, which is not in the 95% region of acceptance: [-2.0096 : 2.0096].

$\bar{x} = -0.009$, is not in the 95% region of acceptance: [-0.005078 : 0.005078].

The standard deviation of the difference, S' equals 0.00253, is used to calculate the statistic.

4. Effect size

The observed effect size d is **medium, 0.5**. This indicates that the magnitude of the difference between the average and μ_0 is medium.

If you like the page, please share or like. Questions, comments and suggestions are appreciated. (statskingdom@gmail.com)

Like 51 Share

